A Sensitive Optical Polarimetric Imaging Technique for Surface Defects Detection of Aircraft Turbine Engines

G. C. Giakos, L. Fraiwan, N. Patnekar, S. Sumrain, G. B. Mertzios, and S. Periyathamby

***Abstract*—The design of an optical polarimetric imaging system, aimed to detect cracks or structural defects on the surface of rotating aircraft engine shafts, is presented. The experimental results clearly indicate that high signal-to-noise ratio signals can be obtained, so that it minimizes the use of processing techniques.**

***Index Terms*—High contrast resolution, high signal-to-noise ratio (SNR), optical imaging, polarimetry, polarimetric detection.**

I. Introduction

SURFACE texture-imaging covers a considerable range of techniques of investigation of varying levels of sophistication which are applicable in many industrial and aerospace situations. The real-time imaging of cracks on surfaces under dynamic conditions is very important in many industrial processes.

Pulse beams of ultrasound, typically 0 to 25 MHz, can be used in a number of applications for the inspection and characterization of materials and engineering systems. Incident pulses pass through the sample and are reflected from internal interfaces and local flaws such as cracks, disbonds and lamellar inclusions, with the reflected signals being reflected via various scan methods. Due to the availability of time-of-flight information and full waveform capturing capabilities, features can be located in three dimensions. Ultrasonics is ideal for the detection of surface defects such as cracks, voids and inclusions, carbon composites for aging or impact damage, as well as bulk properties such as porosity. Ultrasonics can be applied to metal components as well as carbon composites and ceramics. The main limitations of ultrasound waves consist on the fact that a high-resolution scan of large parts can take many hours (acquisition frequency nearly 1000 data points per second).

Infrared imaging is a global area inspection technique that detects and measures temperature and temperature differences to detect indications of disbond, delamination, cracks, corrosion metal loss, residual stress, and other conditions and impact heat flow. Standard methodologies use infrared thermography to measure apparent surface temperature patterns, some of which depict subsurface defect sites. It is difficult to distinguish the defect sites from the noise produced by surface emissivity variations. Interpretation of interior defect sites from metal structures is particularly difficult. Emissivity-corrected IR thermography utilizes the emissivity ratio at two different IR wavelengths to remove emissivity noise and enhance surface temperature contrast. The spatial resolution of this technique is rather limited. On the other hand, optical pyrometric systems, aimed to ensure optimized engine performance, offer the advantages in detecting the spatial and time-varying temperature distribution of fast rotating components with a high resolution.

Several other imaging applications have been explored for nondestructive imaging. For instance, high-speed time-resolved holographic imaging, originally developed for investigation of shock fronts in dispersed particle explosives, can be utilized to understand the mechanics of high-speed growth cracks in brittle materials. Conventional radiography relies on the generation of images corresponding to density, atomic number, and thickness variation of static, solid objects. This technique has limitations in the sense that laminations, narrow cracks, or cracks parallel to the film plane are not readily discernible. On the other hand, real-time radiography offers dynamic range and resolution not as good as those images produced on classical film radiography. However, recent advances in scanning imaging detectors lead to further improvements [1], [2].

In this study, the design of a high signal-to-noise ratio (SNR) optical system, operating on polarimetric detection principles, aimed to detect cracks and structural defects on the surface of rotating aircraft engine shafts, is presented [3]–[5]. Experimental results leading to an improved SNR are presented. Also, several noise components associated with the detected signals have been reduced by applying suitable wavelet transforms. Interestingly enough, Fourier systems and transforms are not well adapted to the local analysis of a function in the time or space domain, since a local perturbation in $f(t)$ may significantly affect all Fourier coefficients $\hat{f}(n)$.

A detailed study of the applied wavelet denoising techniques is described in another author's contribution.

II. Polarimetric Imaging

Optical imaging techniques are preferred because the process is noncontacting and the process is not destructive to the surface. In this study, a polarimetric imaging technique for detection of cracks and surface anomalies of rotating aircraft engines is proposed.

Manuscript received March 1, 2003; revised August 20, 2003. This work was supported by NASA NAG3-2632 Research Grant.

G. C. Giakos, L. Fraiwan, N. Patnekar, S. Sumrain, and S. Periyathamby are with the Optical Electronics, Photonic Devices, and Communication Networks Laboratory, Imaging Systems, NanoEngineering and Intelligence Based Sensor Fusion Laboratory, Department of Electrical and Computer Engineering, The University of Akron, Akron, OH 44325 USA (e-mail: giakos@uakron.edu).

G. B. Mertzios is with the School of Applied Mathematical and Physical Sciences, National Technical University of Athens (NTUA), Athens, Greece.

Digital Object Identifier 10.1109/TIM.2003.821497

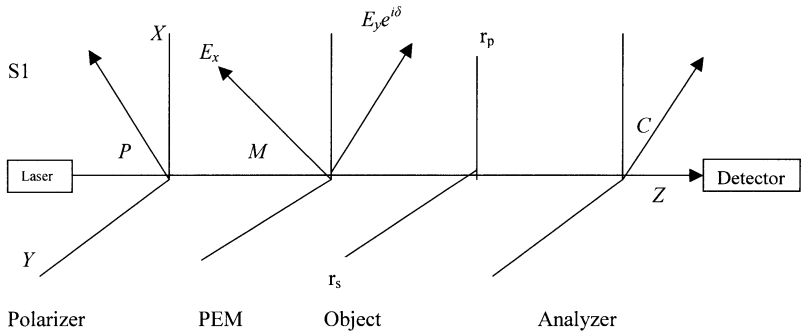

Fig. 1. Optical beam polarization pathway in the experiment setup.

TABLE I

Factors affecting Polarization State of the Scattered Light Radiation
Incident polarization state
Size of the scatterer
Shape of the scatterer
Concentration of the scatterer
Refractive indexes of the scatterer and the surrounding medium

Optical polarimetry is phenomenological in the sense that it concentrates on the resulting properties, which any material with certain fundamental properties will exhibit.

Detection of the weakly scattered light with concurrent rejection of the highly scattered light can yield to improved images, with reduced noise and high contrast. Several methods have been explored to separate weakly scattered and scattered light, such as, time gating, confocal detection techniques, frequency-domain amplitude modulation, polarimetric imaging, and trans-illumination laser-computed tomography. Recently, there as been considerable interest in applying the polarization state of light as discrimination criterion. Polarimetric imaging techniques rely on the assumption that weakly scattered light maintain its initial polarization state, while high scattering light does not maintain it. In general, the polarization of the scattered light depends upon a number of geometrical and physical parameters, as shown in Table I.

Interestingly enough, one can observe a large variety of intensity patterns by varying the polarization state of the incident laser light and changing the analyzer configuration to different polarization components of the backscattered light.

Polarimetric sensing and imaging detect the presence in the state of polarization of the light [6]–[11], [20]. Unlike reflection from dielectrics, reflection of linearly polarized light from a metal surface does not, in general, yield linearly polarized light. Linear polarized light incident on a crack will be reflected. Each reflection will contain a certain polarization state with a certain phase difference with respect to the incident light. Therefore, a phase-contrast imaging technique can be established. The theory of the polarimetric imaging can be explained theoretically in terms of Jones and Mueller matrix methods [6]–[9], [20]. Both are useful in problems involving polarizers and retarders and the Mueller calculus can also be employed in problems involving scatterers. In one respect, the Mueller calculus can be considered more generally applicable than Jones calculus because it can treat partially polarized light as well fully polarized light. Another possible advantage of the Mueller calculus is that it is more directly applicable to experimental measurements [20].

Equivalently, the Mueller method is specified in terms of intensity, which is observable in the laboratory, while the Jones vector is specified by the amplitude and phase of the electric field vector [6]–[9], [10]. Polarimetry has become an indispensable tool in modern electromagnetic sensor technology both in the civil and the military sectors and also in remote sensing [8]-[11]. Generally, Stokes or Mueller calculus can be used to calculate the theoretical expression of the light intensity of a monochromator light beam emerging from the sequence of optical elements, including the polarizer, the photoelastic modulator (PEM), the cylinder and the analyzer. Recently, it started to attract the interest of the scientific community for biomedical optical applications and physiological imaging [11]–[19].

III. Polarimetric Technique

The experimental geometry of the proposed polarimetric technique is shown, in Fig. 1.

A 100-mW, 633-nm HeNe coherent light beam is produced using Melles–Griot laser system. This beam is made linearly polarized by Glenn Thompson polarizer at 45° from the PEM axis. The photo elastic modulator PEM-90 consists of a rectangular fused silica block cemented to a piezoelectric quartz crystal oscillating at the frequency of 50.17 kHz. A uniaxial sinusoidal standing wave is established in the fused silica block and induces a time-varying birefringence. This generates a periodic relative phase shift δ between the orthogonal amplitude components the transmitted beam. This relative phase shift has the form

$$\delta = A \sin \omega t \tag{1}$$

where ω is the resonant angular frequency, in rad/s, of the modulator unit and A, in radians, is the modulation amplitude. A is proportional to the excitation voltage applied to the crystal and the light wave number.

An adjustable slit is used to control the beam width before illuminating the object under investigation. The state of light polarization is changed continuously using the photo elastic modulator. The light changes between vertically and horizontally polarized light at the frequency of $\mathrm{f} = 50.17$ kHz. The state of polarization of the incident light will change according to

the optical properties of the surface. The reflected light will be generally elliptically polarized. The state of polarization is analyzed by a second linear polarizer aligned at -45 of the PEM. A high-sensitivity New Focus photo detector of 200-kHz bandwidth detects the light emerged from the polarizer. The signal from the detector is analyzed using a signal conditioner to separate the ac and dc components of the signal. The lock-in amplifier is used to determine the different harmonics of the detected signal at f and 2f, the reference frequencies for the PEM controller.

Overall, the detected light intensity takes the general form

$$I(t) = I_o + I_s \sin[\delta(t)] + I_c \cos[\delta(t)] \tag{2}$$

where

$$I_o = \frac{\left|r_p^2 + r_s^2\right|}{4}(1 + \cos 2C \cos 2M \cos 2(M-P) - (\cos 2C + \cos 2M \cos 2(M-P) \cos 2\Psi) \tag{3}$$

$$I_s = \frac{\left|r_p^2 + r_s^2\right|}{4}(-2 \sin 2(M-P) \sin 2C \sin 2\Psi \sin \Delta) \tag{4}$$

$$I_c = \frac{\left|r_p^2 + r_s^2\right|}{4}(-2 \sin 2(M-P)(\sin 2M(\cos 2\Psi - \cos 2C) + \cos 2M \sin 2A \sin 2\Psi \cos \Delta)) \tag{5}$$

where ψ and Δ are the ellipsometric angles defined by the complex reflectance ratio

$$\rho = \frac{r_p}{r_s} = \tan \Psi \exp(i\Delta) \tag{6}$$

$$\Delta = \phi_p - \phi_s \tag{7}$$

$$\tan(\Psi) = \left|\frac{r_p}{r_s}\right|. \tag{8}$$

The subscripts p and s refer to the plane wave electric field components that are parallel and perpendicular to the incidence plane, respectively. P, M, and C are the orientation angles for the polarizer, PEM and analyzer, respectively.

Interestingly enough, the PEM introduces a variable retardation δ at a resonant frequency of ω. As a result, the polarization states of the exiting laser beam oscillates between right and left circular polarization states. The retardation varies as a function of time at a frequency f and can be given by

$$\delta = \mathrm{A} \sin(\omega t) \tag{9}$$

where δ_0 is the peak amplitude of retardation and can be controlled by the experimenter.

Based on (9), the Fourier series expansions of $\sin \delta$ and $\cos \delta$ are

$$\sin \delta = 2 \sum_{m=0}^{\infty} J_{2m+1}(A) \sin[(2m+1)\omega t]$$

$$\cos \delta = J_o(A) + 2 \sum_{m=0}^{\infty} J_{2m}(A) \cos[(2m+1)\omega t] \tag{10}$$

where $\mathrm{J_m(A)}$ is the Bessel function of argument A and order m.

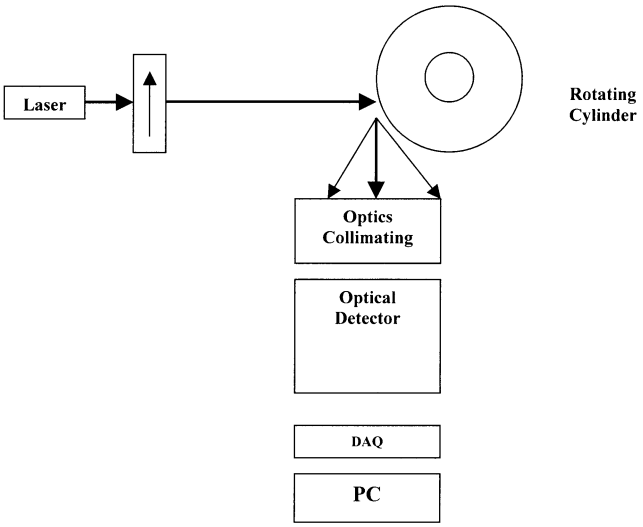

Fig. 2. Light intensity detection experimental setup.

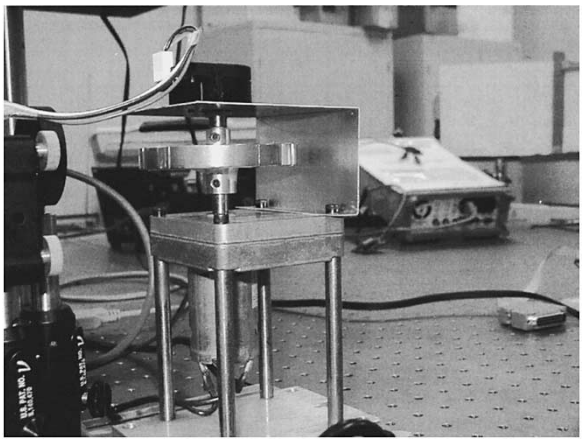

Fig. 3. Experimental rotating phantom prototype.

The detected light intensity is given by

$$I(t) = I_o + J_o(A) I_c + 2I_s \sum_{m=0}^{\infty} J_{2m+1}(A) \sin[(2m+1)\omega t] + 2I_c \sum_{m=0}^{\infty} J_{2m}(A) \cos[(2m+1)\omega t]. \tag{11}$$

A ratio circuit is used to normalize the detected harmonics with respect to the dc components, according to

$$I_{1f} = \frac{2J_1(A) I_s}{I_o + J_o(A) I_c} \tag{12}$$

$$I_{2f} = \frac{2J_2(A) I_c}{I_o + J_o(A) I_c} \tag{13}$$

IV. Experimental Setup and Results

A. Light Intensity Detection and Wavelet Denoising

Initially, an experiment was conducted based on light intensity detection. The experimental setup is shown in Fig. 2. A rotating cylinder with three wires with different diameters, namely 0.254 mm, 0.127 mm, and 0.1 mm, was used to simulate the cracks (Fig. 3). A 10-mW, 633-nm laser beam hits the cylinder, and the reflected light intensity is recorded, as

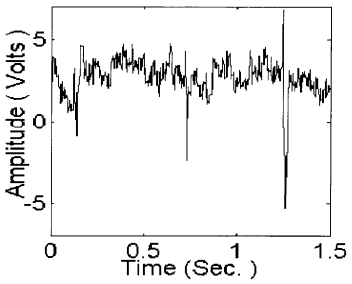

Fig. 4. Detected light intensity for three wires of diameter 0.254 mm, 0.127 mm, and 0.1 mm.

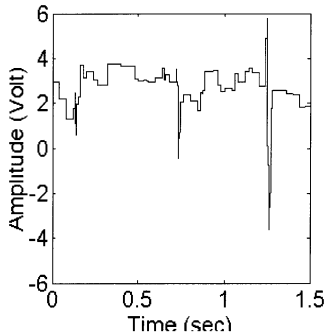

Fig. 5. Signal post-processing for noise removal utilizing Matlab wavelet transform.

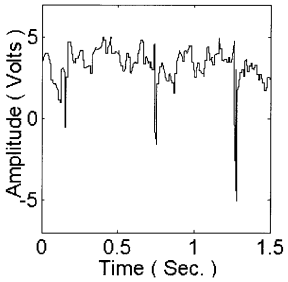

Fig. 6. Real-time denoising utilizing wavelet transform implemented by FPGA.

shown in Fig. 4. The detected signal was either denoised using a real-time wavelet transform system implemented by a field programmable gate array (FPGA) (Fig. 5), or post-processed through a Matlab wavelet transform denoising algorithm. Both the results of the Matlab-based wavelet noise removal post-processing technique and the real-time FPGA-based processing technique are shown in Figs. 6 and 7, respectively. The descriptions of the FPGA-based processing as well as the applied wavelet denoising techniques are described in a companion paper.

B. Polarimetric Detection Technique

The presented polarimetric imaging technique is shown in Fig. 7. A rotating cylinder with different diameter wires was used. The cylinder surface was scanned using the proposed technique. The laser source employed in this study was a 633-nm wavelength Melles–Griot high-performance diode laser 56ICS. It has a high power stability that makes it suitable for this type of study, which requires long time acquisitions.

The PEM has a transducer-optical element assembly, the optical head and the electronic head. The optical head consists of a rectangular window of optical element bonded to a quartz piezoelectric transducer. Both the optical element and the transducer are tuned to the same frequency. When connected to a driver circuit, this assembly oscillates and produces the time-varying optical retardation. The driver circuit consists of an active LC tank circuit connected in parallel to the optical assembly. The driver circuit receives 24-V power, a dc current signal that establishes the peak retardation level, and a feed-forward current signal that stabilizes the peak retardation at the designated value.

The main function of the PEM controller is to control the peak retardation setting of the modulator. Other functions include digital display of the PEM parameters. The PEM provides external interface and reference signals at the operating frequency, 50.17 kHz, and twice the operating frequency, 100.34 kHz.

The lock-in amplifier employed in this study is Stanford Research Systems model SR-830 DSP. Lock-in amplifiers are used to detect and measure very small AC signals. The SR-830 measures the amplitude and the phase of the signal simultaneously. It has a digital signal processor with a 4–16-bit ADC that provides high-precision measurements. The DSP processor provides a unique detection system that uses different techniques for the best performance. It has high sensitivity and can detect a very weak signal of the order of nanovolts. The bandwidth of this lock-in amplifier is 2 mHz–102 kHz, which includes the range of our measurements.

The SR-830 multiplies the input signal by pure sine waves at the reference frequency (supplied by the PEM-90 controller). All frequency components of the input signal are multiplied by the reference simultaneously. Sine waves of different frequencies are orthogonal, i.e., the average of the two frequencies is zero unless the two frequencies are the same. As a result, the product of this multiplication yields a dc output signal proportional to the component of the signal whose frequency is exactly locked to the reference frequency. The low-pass filter, which follows the multiplier, provides the averaging that removes the products of the reference with components with other frequencies.

The SR-830 is supplied with a built-in ratio circuit that was used in this study for normalizing the ac component of the signal to the dc component.

Different detectors were tested for best results, and the most appropriate detector that met the requirements of the proposed setup is NEW FOCUS 2001-FS. This detector has many features including shot noise-limited performance, which makes it suitable for use with a lock-in amplifier, moderate bandwidth of dc-200 kHz, which is the range of our measurements, low noise, and high responsivity which makes it capable of detecting very weak signals.

The normalized first and second harmonics of the detected signal are shown in Figs. 8 and 9, respectively. As an additional step, different wires of diameter of 0.1016, 0.1143, 0.160 02, 0.2032, 0.254, and 0.3048 mm were fixed on the cylinder phantom. The detected signal using the standard light intensity technique is shown in Fig. 10. For the polarimetric detection system, two signals were detected: the first harmonic signal at 50.17 kHz, shown in Fig. 11, and the second harmonic at

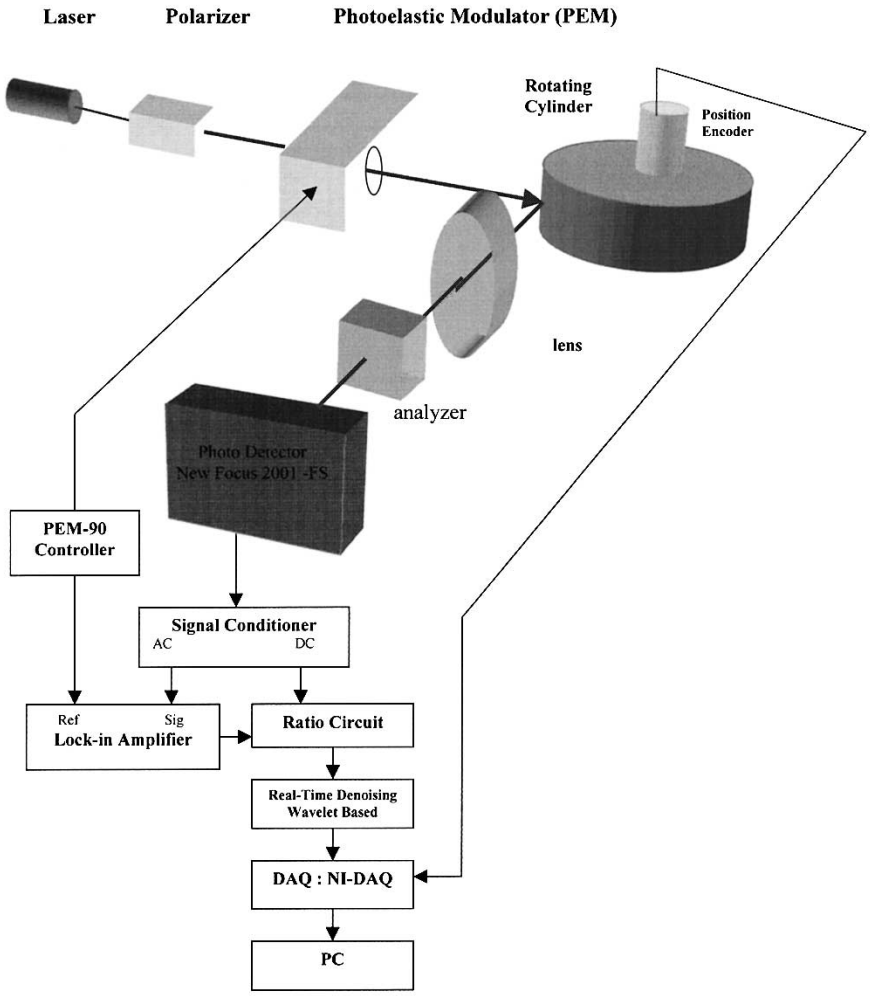

Fig. 7. Polarimetric detection experimental setup.

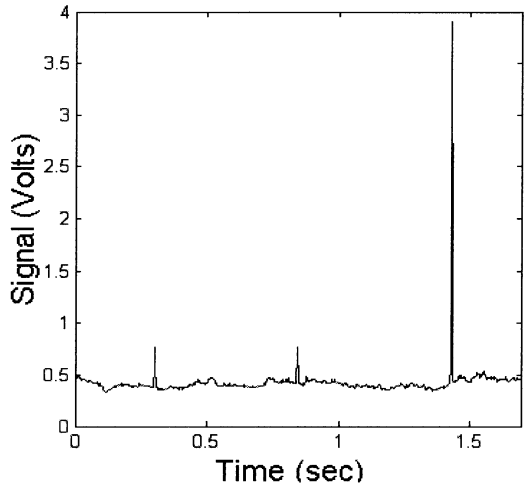

Fig. 8. Normalized first harmonic component, 50.17 kHz, of the detected signal for three wires of diameter 0.254 mm, 0.127 mm, and 0.1 mm.

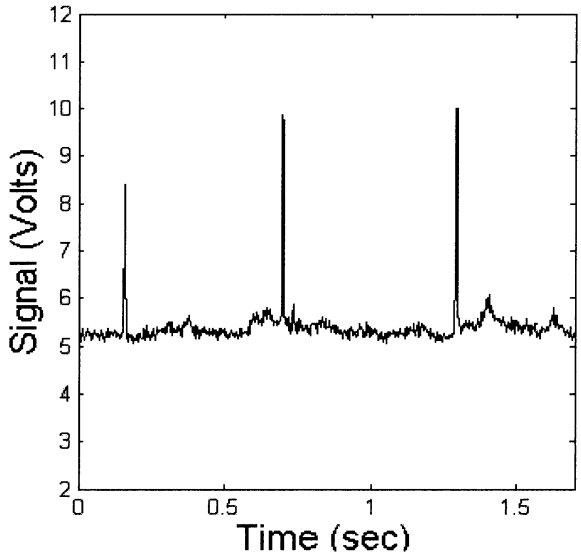

Fig. 9. Normalized second harmonic component, 100.34 kHz, of the detected signal for three wires of diameter 0.254 mm, 0.127 mm, and 0.1 mm.

100.34 kHz signal, shown in Fig. 12. As shown in Figs. 11 and 12, the first harmonic has less noise than the second one. This is related to the bandwidth of different components of the experiment setup. Between the two light detection techniques, the polarimetric detection system produced the best signal. The two harmonics enable double-channel measurements for the object under investigation. Interestingly enough, the second harmonic produces a stronger signal for small wires. A t-test was

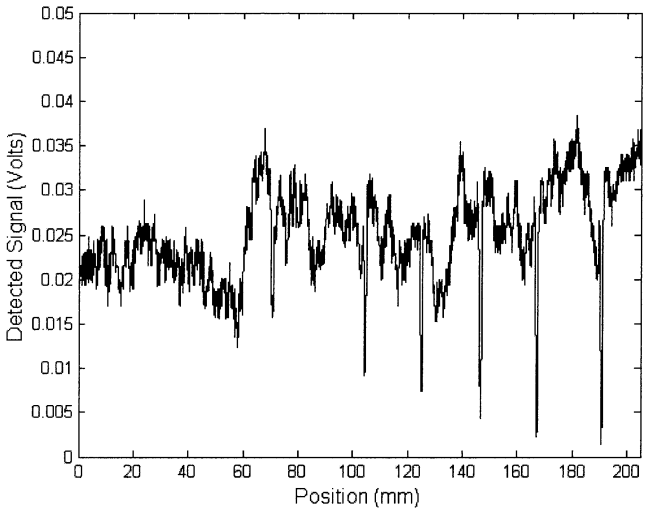

Fig. 10. Detected signal using light amplitude detection technique for different wires of diameter of 0.1016, 0.1143, 0.160 02, 0.2032, 0.254, and 0.3048 mm.

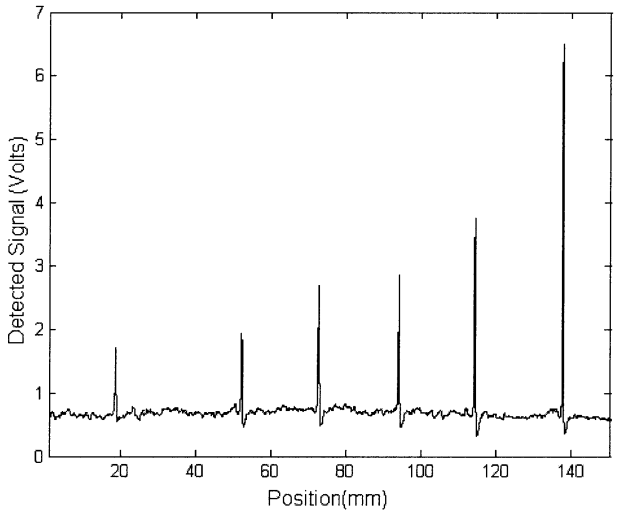

Fig. 11. Normalized first harmonic signal, 50.17 kHz, of the detected signal, for different wires of diameter of 0.1016, 0.1143, 0.160 02, 0.2032, 0.254, and 0.3048 mm using polarimetric detection technique.

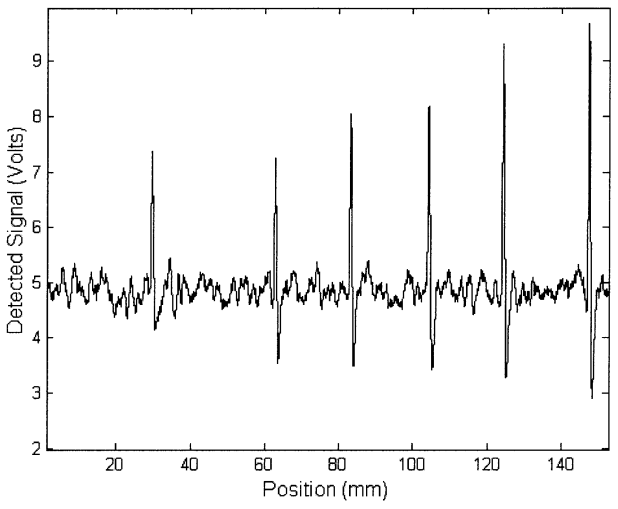

Fig. 12. Normalized second harmonic signal, 100.34 kHz, of the detected signal, for different wires of diameter of 0.1016, 0.1143, 0.160 02, 0.2032, 0.254, and 0.3048 mm, using polarimetric detection technique.

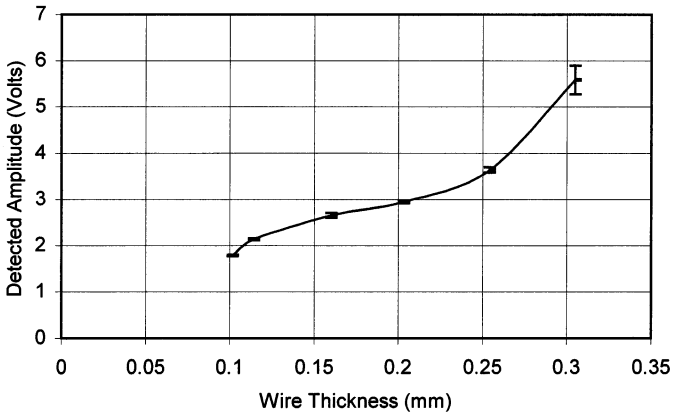

Fig. 13. Measured system responsivity, at different wire thicknesses, first harmonic (50.17 kHz).

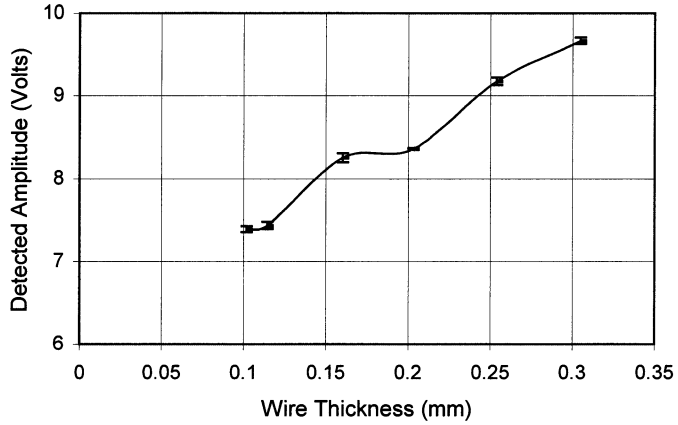

Fig. 14. Measured system responsivity, at different wire thicknesses, second harmonic (100.34 kHz).

performed between the smallest wire signal amplitude and the signal of the cylinder surface, the base signal. The t-test showed that there is a significant difference between the two signals. The null hypothesis was rejected, and the alternative hypothesis of significant difference was accepted.

The system responsivity for the first and second harmonic signals is shown in Figs. 13 and 14, respectively. The two plots of Figs. 13 and 14 indicate that the polarimetric detection system provides different output voltage for different thickness wires. Increasing the wire thickness, the input line spread function increases the output voltage of the two harmonics, because of the larger integration time. Furthermore, by relating the integration time to the linear velocity of the rotating shaft, information regarding the wire width can be obtained.

Overall, polarimetric imaging showed better results than traditional light intensity and phase detection techniques. Optical polarimetric imaging showed a significant improvement in the ability to detect surface discontinuities. The first and second harmonic signals provide a dual source of information about the optical object under investigation. The first harmonic signal provides a better contrast to discriminate between discontinuities in the surface and has less noise, while the second harmonic has more noise. The second harmonic signal is detected at 100.34 kHz, which is at the limit of the detector bandwidth and the lock-in amplifier. The detector has a bandwidth of 200 kHz

at a gain of one, while it has a bandwidth of 20 kHz at maximum gain.

V. Conclusion

In this study, the design of a high-efficiency optical polarimetric system for imaging of cracks and structural defects of a rotating metallic shaft is presented. The use of the presented polarimetric imaging technique renders unnecessary the use of processing imaging techniques.

References

[1] G. C. Giakos, "Multidensity and multiatomic number detector media with gas-electron multiplier, for imaging applications," U.S. patent 6 316 773, Nov. 13, 2001.
[2] ——, "Multidensity and multiatomic number detector media for applications," U.S. patent 6 069 362, May 30, 2000.
[3] ——, Development of an optical-real-time polarimetric imaging system for aerospace applications, in NASA Research Grant NAG3-2632, 2001.
[4] G. C. Giakos, L. Fraiwan, N. Patnekar, S. Sumrain, J. Carletta, and F. Krach, "An optical polarimetric system for surface defect detection of aircraft engines," in *Proc. IEEE Instrumentation and Measurements Technology Conf.* , Anchorage, AK, 2002, pp. 1701–1704.
[5] L. Fraiwan, "An Efficient Technique for High Reflectivity Polarimetric Imaging System with Real Time Denoising," M.S thesis, Univ. Akron, Akron, OH, Aug. 2002.
[6] D. S. Kliger, J. W. Lewis, and C. E. Randal, *Polarized Light in Optics and Spectroscopy*. San Diego, CA: Academic, 1990.
[7] K. D. Moller, *Optics*. Mill Valley, CA: University Science Books, 1988.
[8] W. M. Boerner, "Polarization utilization in electromagnetic inverse scattering," *Inverse Scattering Problems Opt.*, vol. 2, July 1980.
[9] E. Collett, *Polarized Light*. New York: Marcel-Dekker, 1993.
[10] D. Giuli, "Polarization diversity in radar," *Proc. IEEE*, vol. 74, no. 2, pp. 245–269, Feb. 1986.
[11] G. C. Giakos, "Book review: Noise and clutter rejection in radars and imaging detectors," *IEEE Antenna Propagat. Soc. Mag.*, June 1993.
[12] S. G. Demos and R. R. Alfano, "Optical polarization imaging," *Appl. Opt.*, vol. 36, pp. 150–155, 1997.
[13] S. L. Jacques, J. R. Roman, and K. Lee, "Imaging superficial tissue with polarized light," *Laser Surgery Med.*, vol. 26, pp. 119–129, 2000.
[14] S. L. Jacques and K. Lee, "Polarized video imaging of skin," in *SPIE Proc. Catanous Applications of Lasers: Dermatolgy, Plastic Surgery, and Tissue Welding*, San Jose, CA, Feb. 26–28, 1998.
[15] J. R. Mourant, A. H. Hieshler, J. P. Freyer, T. M. Johnson, and A. A. Eick, "Scattering properties of biological cells," in *OSA Spring Topical Meet.*, Orlando, FL, Mar. 8–11, 1998.
[16] C. Feng, Y. Huang, J. Chang, M. Chang, and D. Chou, "A true phase sensitive optical heterodyne polarimeter on glucose concentration measurement," *Opt. Commun.*, vol. 141, pp. 314–321, 1997.
[17] R. McNichols and R. Cote, "Optical glucose sensing in biological fluids: An overview," *J. Biomed. Opt.*, vol. 5, no. 1, pp. 5–16, Jan. 2000.
[18] W. S. Bickel, J. F. Davidson, D. R. Huffman, and R. Killson, "Application of polarization light effects in light scattering: A new biophysical tool," in *Proc. Nat. Acad. Sci.*, vol. 73, 1997, pp. 486–490.
[19] R. R. Anderson, "Polarized light examination and photography of the skin," *Arch. Dermatol.*, vol. 127, pp. 1000–1005, 1991.
[20] D. H. Goldstein and R. A. Chipman, "Polarization analysis and measurement," in *Proc. Soc. Photo-Opt. Instrum. Eng.*, vol. 1745, 1992.

G. C. Giakos, photograph and biography not available at the time of publication.

L. Fraiwan, photograph and biography not available at the time of publication.

N. Patnekar, photograph and biography not available at the time of publication.

S. Sumrain, photograph and biography not available at the time of publication.

G. B. Mertzios, photograph and biography not available at the time of publication.

S. Periyathamby, photograph and biography not available at the time of publication.